These note are meant to be a supplement to Chapter 13 of the text, but not a replacement for it.

1 Introduction

The idea of large-eddy simulation as well as the first simulations came out of the atmospheric science community in the 1960's. Numerical simulations were under develop for weather prediction. In the simulations the numerical resolution only allowed grid spacing in the kilometers, at best. An important issue was how to treat the motions below the grid scale. This can be seen in Figure 1, which is a typical plot of the absolute vorticity over the Pacific Northwest and surrounding areas. It is easy to understand that, even with the top high performance computers available today, motions on length scales below a few kilometers must be parameterized. Developing parameterizations for the below grid scale (subgrid-scale, or residual) motions is the basic idea behind large-eddy simulation.

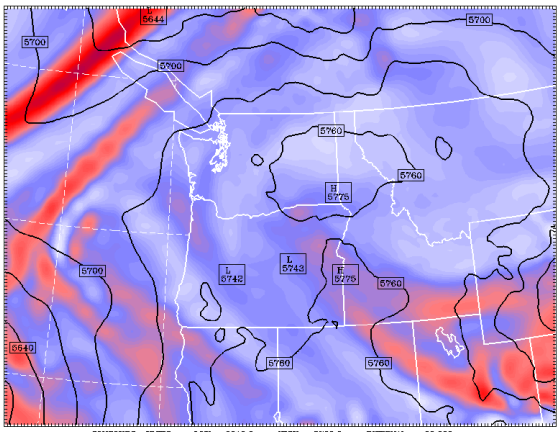

Figure 1: Absolute vorticity in a typical weather prediction.

1.1 History

In the late 1940's and 1950's,m people like Jule Charney and John von Neumann were leading the way in using computers to predict weather. A key issue was how to treat the subgrid-scale motions, both in terms of modeling them, but also in terms of adding diffusion or viscosity to stabilize the simulations. They drew on work that was done on gas dynamics and on turbulence modeling at the time. Then in 1963 Joe Smagorinsky (*Mon. Weath. Rev.*, **91**(3):99) suggested a model to treat the subgrid-scale diffusion/viscosity effecting the larger-scale, quasi-two-dimensional motions in the atmosphere. The model was based upon Prandtl's mixing length ideas. Doug Lilly was a atmospheric scientist at the Princeton Geophysical Fluid Dynamics Laboratory working with Smagorinsky, and took a position at the National Center for Atmospheric Research (NCAR) in the mid 1960's. He published a paper in 1967 (*Proc. IBM Sci. Comp. Symp. on Environ. Sci.*, IBM Form no 320-1951, 195) that suggested extending Smagorinsky's ideas to simulating turbulence. He also showed how to compute the free coefficient in the model consistent with Kolmogorov's theory of the inertial subrange. Jim Deardorff had joined Lilly's group in the late 1960's picked up on Lilly's ideas and performed the first large-eddy simulations. He presented his results at a

Boeing Symposium in Seattle in 1969, and published them in 1970 (*J. Fluid Mech.*, **41**(2):453). His interest was in the atmospheric boundary layer, but the simulations were of a turbulent channel flow. Using the best computers available at the time, his simulations used 24x14x20 grid points, so that now the simulations would probably be called a 'very large-eddy simulation'.

Within the next year, Stu Patterson and Steve Orszag, both visitors at NCAR, performed the first direct numerical simulations. Later Deardorff published a series of papers in the 1970's based upon large-eddy simulations of the atmospheric boundary layer which had an important impact on understanding and modeling of this flow. Research employing large-eddy simulations has continue up to today at NCAR, and in the atmospheric sciences community at several locations.

Meanwhile, Hans Mark, who was the technical director of NASA Ames in the 1970's, started a large program there on the simulation of turbulence. (The Illiac computer was at NASA Ames at the time, one of the most powerful computers in the world. CDC and Cray computers were at NCAR.) This program was continued, especially at nearby Stanford, at the NASA/Stanford Center for Turbulence Research.

Large-eddy simulation is now being used at many places world-wide, with research on many topics, e.g., turbulent reacting flows, turbulent supersonic flows, etc., and is working its way into even commercial computer codes. The growth in the use of large-eddy simulation in the study of turbulence can easily be seen by examining the number of publication with 'large-eddy simulation' in the title and/or abstract of papers in the Science Citation Index.

1.2 Some references

The following are some useful references on the topic of large-eddy simulation. In addition to what is listed, there are a number of review papers on special topics (applications), and probably some books not mentioned.

- Our text, chapter 13. This is a very good introduction to the topic, hitting on most of the important key issues.
- Pierre Sagaut, 2002, 'Large eddy simulation for incompressible flows', 2nd edition, Springer. This is a good reference; it is very detailed, but also very math oriented.
- Marcel Lesieur et al., 'Large eddy simulations of turbulence', Cambridge University Press, 2005. This is written by users, and for users.
- Bernard Geurts, 2003, 'Elements of direct and large-eddy simulation'.
- M. Lesieur & O. Métais. 1998. 'New trends in LES of turbulence', *Annu. Rev. Fluid Mech.*, **28**: 45.
- C. Meneveau & J. Katz, 2000, 'Scale invariance and turbulence models for LES', *Annu. Rev. Fluid Mech.*, **32**: 1.
- P. Moin, 2002, 'Advances in large-eddy simulation methodology of complex flows', *Int. J. Heat & Fluid Flow*, **23**(5):710.
- many more on specialized topics.

1.3 Definition

Large-eddy simulation (LES) of turbulence: the numerical solution of the large-scale, three-dimensional, time-dependent motions. The smaller scale motions are modeled. Appropriate initial and boundary conditions must be satisfied.

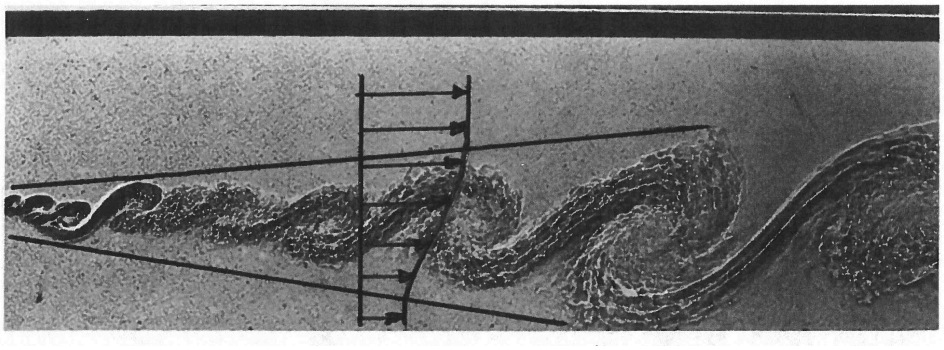

Figure 2: Large-scale structure in a turbulent shear layer.

Consider the turbulent shear layer depicted in Figure 2. It is taken from an experiment in which spark shadow is used to give an almost instantaneous view of the flow (from the thesis of J. H. Conrad, Caltech, 1976). What is apparent is the broad range of length scales in the flow, which could be difficult if not impossible to resolve in a numerical simulation, depending on the Reynolds number of the flow. Also in the figure is a sketch of the mean velocity profile for this flow, something that would be predicted by a model using the Reynolds-averaged Navier-Stokes (RANS) equations. RANS modeling has no direct information about the large-scale structures that are clearly seen in the figure. If some phenomenon, e.g., chemical reaction, depended on these structures, then the RANS approach would have difficulty in accurately predicting such phenomena. Large-eddy simulation, however, would be directly computing these large-scale motions, presumably giving a much better prediction of the phenomena.

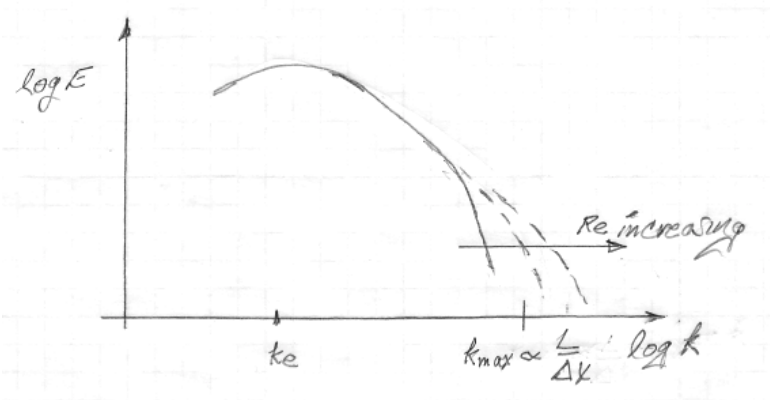

Figure 3: Cartoon of energy spectrum showing how it increases with the Reynolds number.

Assume that the one-dimensional energy spectrum for this flow is like what is displayed in the sketch in Figure 3. In the figure, k_e in the wave number characterizing the energy-containing range, and k_{max} is the numerical cut-off wave number, inversely proportional to the grid spacing

Δx. Using high performance computers, grid points of number $1,000^3$ are common now, with a few simulations in the range of $10,000^3$. For the solid curve, characterizing a lower Reynolds number flow, the entire energy spectrum can be resolved in a simulation, and it would be possible do conduct direct numerical simulations for this flow. The range in wave number requiring resolution goes approximately as the ratio of the Kolmogorov wave number k_K to k_e. As the Reynolds number is increased, this ratio grows as $k_K/k_e \propto Re^{3/4}$, so that the resolution requirements become extremely severe as the Reynolds number is increased. At some point, typical of most applications, the spectrum cannot be resolved.

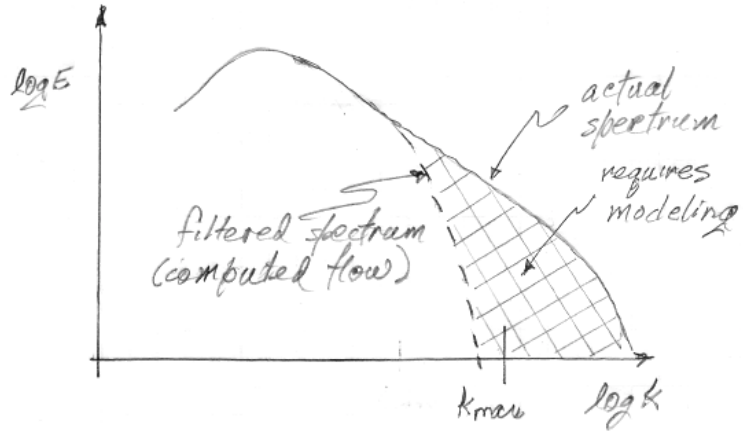

Figure 4: Cartoon depicting the equilibrium range.

This suggests the computational approach shown in Figure 4. Setting k_{max} to be as large as possible for a particular simulation (choosing Δx to be as small as possible),

1. the dynamical equations are filtered, resulting in a smooth field for which accurate simulations can be performed;

2. the effects of the part that is filtered out, the 'subgrid-scale', or residual motionss, are modeled;

3. the simulations are carried out for the 'grid-scale' motions, i.e., the large-eddies;

4. the statistics are obtained by averaging over the computed flow fields as in DNS (but care must be take in include the subgrid-scale motions in the averaging).

1.4 Advantages of large-eddy simulation

The approach of large-eddy simulation has some major advantages and disadvantages. Among the advantages are the following.

- The large-scale (energy-containing) motions are directly computed (not modeled). Motions at the large scale generally control the dynamics of the turbulent flow (even the kinetic energy dissipation rate at the small scales, which depends on the energy transfer rate from the large scales). The large scale motions cause the most difficulty in RANS modeling. All the large-scale fluctuating motions must be modeled. They vary significantly from flow-to-flow, however, suggesting that different modeling might be needed from flow-to-flow.

- In large-eddy simulation, only the small scales are modeled. These scales generally have little energy (generally 5% or less of the turbulent kinetic energy) so that there is not as much influence of the modeling. In addition, the smaller scale motions are more 'universal', so that a good small scale model should be applicable for a range of flows.

So in theory large-eddy simulation would be expect to apply to very high Reynolds number flows.

1.5 Disadvantages of large-eddy simulation

There are clearly some disadvantages as well to employing large-eddy simulations.

- Compared to DNS, large-eddy simulation requires some *ad hoc* modeling. This can be especially difficult near boundaries.

- Compared to RANS, the numerical problem for large-eddy simulation is very difficult. The simulation must be three-dimensional and time-dependent. Considerably more resolution in space and time is required than for RANS, with smaller time scales to be resolved (more time steps), and smaller spatial scales to be resolved (more grid points). Generally, to keep the computational size and length manageable, very accurate numerical methods are used in large-eddy simulation.

1.6 General comments

At the present time, large-eddy simulation is used as a research tools, e.g., to explore flows in detail (numerical experiments, as first done by Deardorff), and to develop and improve subgrid-scale modeling, e.g., for chemically-reacting flows, multiphase flows, boundary layer flows.

Currently large-eddy simulation is beginning to be used in applications. This is especially true in situations where RANS is expected to be inaccurate, e.g., for flows with large density variations, for fast rotating flows. In general, however, it is too computationally intensive and too complicated to use. It is starting to appear, however, in commercial codes. But it must be recognized that most (all?) commercial codes are low order codes, which makes numerical resolution in space and time even more difficult.

1.7 Development of the equations for large-eddy simulations

The development of the equations for large-eddy simulations parallels that for the ensemble (or time, etc.) averaged equations, which includes the following steps.

- An averaging operator is defined, in this case a spatial filter (also implying a temporal filter).

- This filtering is then applied to the Navier-Stokes equations, resulting in a closure problem related to the filtered (subgrid-scale, or residual) motions; the closure problem is again due to the nonlinearity in the equations.

- Models are offered for the effects of the subgrid-scale motions, closing the equations.

- Appropriate numerical methods are then used to solve the resulting equations.

2 Filtering

Of interest in large-eddy simulation is the filtered values of the unknowns, e.g., of $\mathbf{U}$ and p. First the filtering operators will be defined, and their properties will be explored. Then, in order to obtain dynamic equations for these filtered quantities, the Navier-Stokes equations are then filtered.

Given an unknown, e.g., $U(\mathbf{x}, t)$, a spatial filtering operator is defined by:

$$\bar{U}(\mathbf{x}, t) = \int G(\mathbf{r}, \mathbf{x}) U(\mathbf{x} - \mathbf{r}, t) d\mathbf{r}\,, \text{ (a convolution)} \tag{1}$$

where

- G is the filter function satisfying
$$\int G(\mathbf{r}, \mathbf{x}) d\mathbf{r} = 1\,,$$
(if this were not true, then the filtered value of a constant would not be that constant), with some implied filtered width Δ, possibly dependent upon $\mathbf{x}$ and related to the grid spacing Δx, and
- the integrals are over the entire (computational) domain, although they are only effective near $|\mathbf{r}| \to 0$.

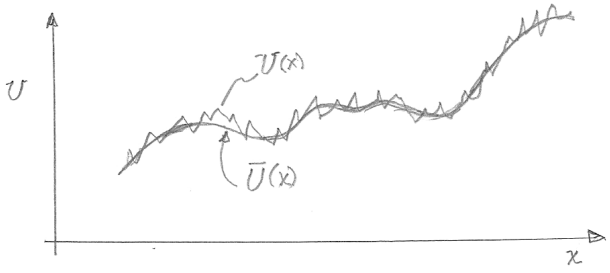

Figure 5: Cartoon of the effect of filtering $U(x)$.

The effect of the filter is qualitatively as shown in Figure 5. Note that, in particular,

$$\begin{aligned} \frac{\partial}{\partial t}\bar{U}(\mathbf{x}, t) &= \frac{\partial}{\partial t}\int G(\mathbf{x}, \mathbf{r}) U(\mathbf{x} - \mathbf{r}, t) d\mathbf{r} \\ &= \int G(\mathbf{x}, \mathbf{r}) \frac{\partial}{\partial t}\bar{U}(\mathbf{x} - \mathbf{r}, t) d\mathbf{r} = \overline{\frac{\partial U}{\partial t}} \text{ (Leibnitz rule),} \end{aligned} \tag{2}$$

assuming that the operations of integration and differentiation can be interchanged.

With $\mathbf{u}'$ called the subgrid-scale motion, and defined by

$$\mathbf{u}'(\mathbf{x}, t) = \mathbf{U}(\mathbf{x}, t) - \bar{\mathbf{U}}(\mathbf{x}, t)\,, \text{ then} \tag{3}$$

$$\overline{\mathbf{u}'}(\mathbf{x}, t) = \bar{\mathbf{U}}(\mathbf{x}, t) - \overline{\bar{\mathbf{U}}}(\mathbf{x}, t)\,. \tag{4}$$

Note that, in general,

$$\overline{\bar{\mathbf{U}}}(\mathbf{x},t) = \int G(\mathbf{x},\mathbf{r})\bar{\mathbf{U}}(\mathbf{x}-\mathbf{r},t)d\mathbf{r} \neq \int G(\mathbf{r},\mathbf{x})U(\mathbf{x}-\mathbf{r},t)d\mathbf{r} = \bar{\mathbf{U}}(\mathbf{x},t)\,.$$

Therefore, in general,

$$\overline{\mathbf{u}'}(\mathbf{x},t) \neq 0\,,$$

which can make the analysis more difficult. We will find that only projection filters, e.g., spectral filters, will have the property that $\overline{\mathbf{u}'}(\mathbf{x},t) = 0$. Also note that

$$\begin{aligned}
\frac{\partial}{\partial x_i}\bar{\mathbf{U}}(\mathbf{x},t) &= \frac{\partial}{\partial x_i}\int G(\mathbf{r},\mathbf{x})\mathbf{U}(\mathbf{x}-\mathbf{r},t)d\mathbf{r} \\
&= \int G(\mathbf{r},\mathbf{x})\frac{\partial}{\partial(x_i-r_i)}\mathbf{U}(\mathbf{x}-\mathbf{r},t)d\mathbf{r} + \int \frac{\partial}{\partial x_i}G(\mathbf{r},\mathbf{x})\mathbf{U}(\mathbf{x}-\mathbf{r},t)d\mathbf{r} \\
&= \overline{\frac{\partial}{\partial x_i}\mathbf{U}(\mathbf{x},t)} + \int \frac{\partial}{\partial x_i}G(\mathbf{r},\mathbf{x})\mathbf{U}(\mathbf{x}-\mathbf{r},t)d\mathbf{r}\,. \qquad (5)
\end{aligned}$$

So spatial differentiation and filtering do not commute unless G is independent of $\mathbf{x}$. In particular, this can lead to additional terms near boundaries since the turbulence scales, and hence the filter width, should decrease as the boundary is approached.

2.1 Types of filters

Several types of filters have been employed in large-eddy simulations. The most commonly used are the following (defined here in one dimension).

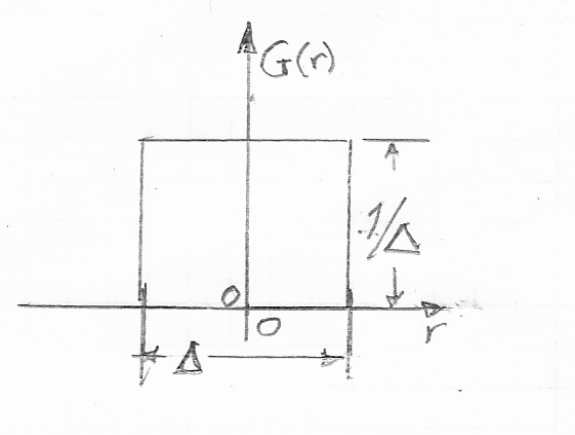

Figure 6: Top-hat filter function $G(r)$.

- top-hat filter (the one originally used by Deardorff). Here the filter is defined by (see Figure 6):

$$G(r) = \frac{1}{\Delta}\begin{cases} 1 & |r| < \frac{1}{2}\Delta \\ 0 & \text{otherwise} \end{cases} \qquad (6)$$

- Gaussian, here defined as (see Figure 7):

$$G(r) = \Big(\frac{6}{\pi\Delta^2}\Big)^{1/2}\exp\Big\{-\frac{6r^2}{\Delta^2}\Big\}\,. \qquad (7)$$

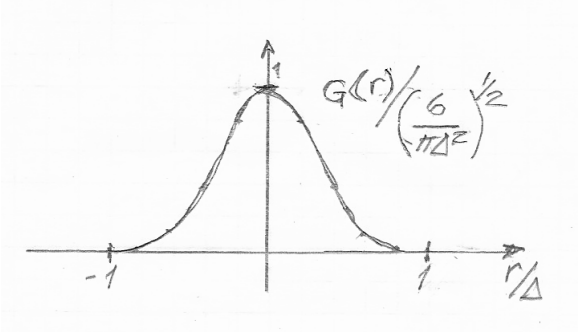

Figure 7: Gaussian filter function $G(r)$.

- The third type of filter is the projection filter. Here we will mainly consider a spectral truncation filter, although various other series, e.g., Chebychev series, could be considered. For a Fourier series with period 2π, a function, say $U(x)$, can be represented as

$$U(x) = \sum_{k=-\infty}^{\infty} \hat{U}_k e^{ikx} .$$

  The spectral truncation filter is then

$$\bar{U}(x) = \sum_{k=-K_c}^{k=K_c} \hat{\bar{U}}_k e^{ikx} \text{ , with } K_c = \pi/\Delta \text{ and}$$

$$\hat{\bar{U}}_k = \begin{cases} \hat{U}_k & |k| < K_c \\ 0 & \text{otherwise} \end{cases}$$

  Note that for this spectral truncation (and projection truncations in general), $\overline{\bar{U}}(x) = \bar{U}(x)$, since the additional truncation does not change $\bar{U}(x)$.

Figure 8 plots all three filters as functions of r. Note that, in physical space, the spectral truncation filter is the Fourier transform of a top-hat filter in wave number space, i.e., the transfer function of the spectral filter. Transfer functions are discussed in the next section.

2.2 Transfer function

In considering any of the filters, if $U(x)$ is representable by a Fourier integral, then in wave number space the filters can be considered as a multiplication of $\hat{U}(k)$ by a transfer function (see Table 13.2, page 563 in the text). Assuming that G is independent of x, then

$$\hat{\bar{U}}(k) = \hat{G}(k)\hat{U}(k) ,$$

where $\hat{G}(k)$ is the Fourier transform of $G(r)$. For the top-hat filter,

$$\hat{G}(k) = \frac{\sin(\frac{1}{2}k\Delta)}{\frac{1}{2}k\Delta} ,$$

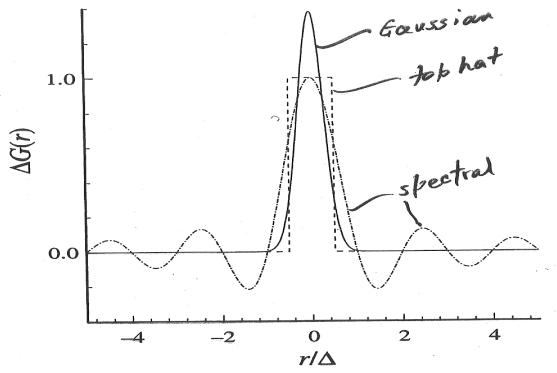

Figure 8: The filters $G(r)$.

which decays in k as $1/(k\Delta)$, which is rather slow and requires more numerical resolution for the filtered function. On the other hand, for the Gaussian filter, probably the most often used in practice,

$$\hat{G}(k) = \exp\Big\{-\frac{k^2\Delta^2}{24}\Big\}\,.$$

Note that the Gaussian filter decays much more rapidly in k than does the top-hat filter, and therefore is more compact and will require significantly less numerical resolution. For the spectral filter,

$$\hat{G}(k) = \begin{cases} 1 & \text{for } k < K_c \\ 0 & \text{otherwise} \end{cases}$$

so that it is compact in wave number space, although not compact in physical space (see Figure 8). The behavior of all three filter transfer functions is shown in Figure 9.

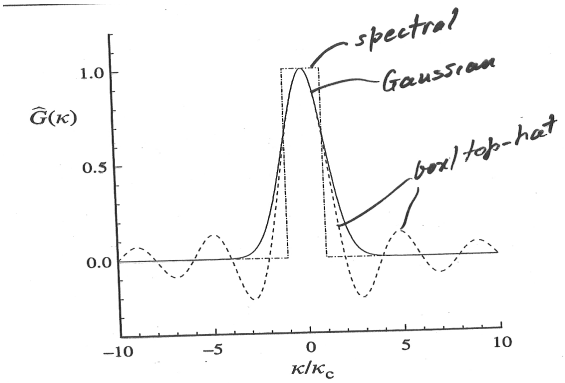

Figure 9: The filter transfer functions $\hat{G}(k)$.

In a homework problem (Problem 13.7, page 570), it is shown that the energy spectrum, for example $E_{11}(k)$ related to the spatial autocorrelation function $\langle u_1(x_1)u_1(x_1+r_1)\rangle$, is related to the energy spectrum of the spatially-filtered velocity as

$$\bar{E}_{11}(k) = |\hat{G}(k)|^2 E_{11}(k)\,.$$

Other properties of the filter functions and filter transfer functions are discussed in the text.

Note the following.

- The grid spacing Δx_g is usually chosen to e a fraction of the filter width, say Δx_f, e.g., $\Delta x_g = \frac{1}{2}\Delta x_f$, so that $K_{cg} \doteq K_{cf}$.
- The numerical scheme will also act as a filter, especially for the top-hat filter case. In fact it can be difficult to totally separate the numerical schemes from the filtering. In the extreme case, the filtering is solely done by the numerical scheme, an approach which is called Implicit LES, which will be discussed later.

2.3 Filtered rate-of-strain

In the following discussion, it will be assumed that G is independent of $\mathbf{x}$ unless otherwise stated. A quantity of importance in modeling, especially in the popular Smagorinsky model, in the filtered strain-rate,

$$\bar{S}_{ij} = \frac{1}{2}\Big(\frac{\partial}{\partial x_j}\bar{U}_i + \frac{\partial}{\partial x_i}\bar{U}_j\Big)\,, \tag{8}$$

and its magnitude

$$\bar{\mathcal{S}} = \Big(2\bar{S}_{ij}\bar{S}_{ij}\Big)^{1/2}\text{, summation on } i,j \tag{9}$$

It is instructive to determine its dependence on the filtering. Assume homogeneous, isotropic turbulence with an inertial subrange. For isotropic turbulence,

$$\langle s_{ij}s_{ij}\rangle = \int_0^\infty k^2 E(k)dk\,,$$

where $E(k)$ is the three-dimensional energy spectrum. (See Equation 6.191, page 222 in the text, noting that $\epsilon = 2\nu\langle s_{ij}s_{ij}\rangle$.) So

$$\langle\bar{\mathcal{S}}^2\rangle = 2\langle\bar{S}_{ij}\bar{S}_{ij}\rangle = 2\int_0^\infty k^2\bar{E}(k)dk = 2\int_0^\infty k^2|\hat{G}(k)|^2E(k)dk$$

(see Problem 13.7, page 570.)

Since k^2 weights the integral towards larger k, but $|\hat{G}(k)|^2$ damps the integrand above $k = K_c$, we expect the maximum contribution to the integral to come from values of k near K_c. But note also that this is where numerical schemes have their greatest errors. If K_c is in the inertial subrange, which is often assumed to be the case of large-eddy simulations, we can use the Kolmogorov inertial subrange spectrum to estimate the integral; i.e., assuming that the principal contribution is due to E near K_c, then $E(k) = C\epsilon^{2/3}k^{-5/3}$, where C is a known constant, so that

$$\begin{aligned}\langle\bar{\mathcal{S}}^2\rangle &\doteq 2\int_0^\infty k^2|\hat{G}(k)|^2C\epsilon^{2/3}k^{-5/3}dk = 2C\epsilon^{2/3}\int_0^\infty k^{1/3}|\hat{G}(k)|^2dk \\ &= 2C\epsilon^{2/3}\Delta^{-4/3}\int_0^\infty(\Delta k)^{1/3}|\hat{G}(k)|^2d(\Delta k) = a_fC\epsilon^{2/3}\Delta^{-4/3}\text{, with}\end{aligned} \tag{10}$$

$$a_f = 2\int_0^\infty \Delta^{4/3}k^2|\hat{G}(k)|^2k^{-5/3}dk = 2\int_0^\infty(k\Delta)^{1/3}|\hat{G}(k)|^2d(k\Delta) \tag{11}$$

which depends on the filter transfer function $\hat{G}(k)$. Note that the integral is independent of Δ, since $\hat{G}(k) = f(k\Delta)$, and furthermore the integral is a constant. An important result is that

$$\langle\bar{\mathcal{S}}^2\rangle^{1/2} \propto \Delta^{-2/3}\,, \tag{12}$$

which will be used below.

The quantity a_f can be easily evaluated. For example, for the spectral truncation filter, with

$$\hat{G}(k) = H(K_c - |k|) = H\Big(1 - \frac{|k|\Delta}{\pi}\Big)\,,$$

with $H(\cdot)$ the Heaviside function, and $K_c = \pi/\Delta$,

$$a_f = 2\int_0^\infty \underbrace{\zeta^{1/3} H(1-\frac{\zeta}{\pi})d\zeta}_{k\Delta=\zeta} = 2\int_0^\pi \zeta^{1/3} d\zeta = 2\frac{\zeta^{4/3}}{4/3}\Big|_0^\pi = \frac{3}{2}\pi^{4/3} \doteq 6.9\,.$$

Note that for a computational grid of length L and N grid points, then $L = N\Delta$, $k_{min} = (2\pi)/L$, $k_{max} = (N/2)k_{min} = (N/2)(2\pi/L) = (N\pi/L) = \pi/\Delta$.

3 Filtering the equations of motion

To obtain the governing equations for the filtered velocity field and pressure field, we filter the Navier-Stokes equations. We assume that the filter G is independent of $\mathbf{x}$ to that the operations of spatial filtering and spatial derivatives commute. We start with the continuity equation, which when filtered gives:

$$\overline{\frac{\partial}{\partial x_i} U_i} = \frac{\partial}{\partial x_i}\bar{U}_i = 0\,. \tag{13}$$

Also, decompositing the velocity into the filtered velocity plus the residual (subgrid-scale) velocity, $U_i = \bar{U}_i + u_i'$, then taking the divergence of U_i and using Equation (13) gives:

$$\frac{\partial}{\partial x_i} u_i' = 0\,. \tag{14}$$

Furthermore, since spatial derivatives and filtering commute, then

$$\overline{\frac{\partial}{\partial x_i} u_i'} = \frac{\partial}{\partial x_i}\overline{u_i'} = 0\,.$$

Next, filtering the momentum equation, after writing the nonlinear term, using continuity, as

$$U_j \frac{\partial}{\partial x_j} U_i = \frac{\partial}{\partial x_j}(U_j U_i)\,,$$

and using the facts that both the time and space derivatives commute with the filtering operation:

$$\frac{\partial}{\partial t}\bar{U}_i + \frac{\partial}{\partial x_j}\overline{U_j U_i} = -\frac{1}{\rho}\frac{\partial}{\partial x_i}\bar{P} + \nu\frac{\partial^2}{\partial x_j^2}\bar{U}_i\,. \tag{15}$$

It is useful to now define the subgrid-scale, or residual, stress as

$$\tau_{ij}^R = \overline{U_j U_i} - \bar{U}_i\bar{U}_j\,. \tag{16}$$

Using Equation (16), Equation (15) can be written as:

$$\frac{\partial}{\partial t}\bar{U}_i + \bar{U}_j\frac{\partial}{\partial x_j}\bar{U}_i + \frac{\partial}{\partial x_j}\tau_{ij}^R = -\frac{1}{\rho}\frac{\partial}{\partial x_i}\bar{P} + \nu\frac{\partial^2}{\partial x_j^2}\bar{U}_i\,. \tag{17}$$

Following what was done with Reynolds stress modeling, it is useful to define a subgrid-scale kinetic energy (an alternative definition, k_r, is given below) as

$$k_{sgs} = \frac{1}{2}\tau_{ii}^R = \frac{1}{2}\overline{U_i U_i} - \frac{1}{2}\bar{U}_i\bar{U}_i \,, \tag{18}$$

so that the anisotropic, deviator part of the subgrid-scale stress tensor is:

$$\tau_{ij}^r = \tau_{ij}^R - \frac{2}{3}k_{sgs}\delta_{ij} \,. \tag{19}$$

Plugging this expression for τ_{ij}^R into Equation (17) gives finally, with

$$\bar{p} = \bar{P} + \frac{2}{3}k_{sgs} \,, \text{ the modified pressure,}$$

$$\frac{\partial}{\partial t}\bar{U}_i + \bar{U}_j\frac{\partial}{\partial x_j}\bar{U}_i = -\frac{1}{\rho}\frac{\partial}{\partial x_i}\bar{p} + \nu\frac{\partial^2}{\partial x_j^2}\bar{U}_i - \frac{\partial}{\partial x_j}\tau_{ij}^r \,. \tag{20}$$

As with the Reynolds averaged equation modeling, we now have 4 equations, Equations (13) and (20) for $\bar{U}_i$ and $\bar{p}$. In addition, however, we have the 6 unknowns τ_{ij}^r so that there is again a closure problem. Note that if the equations were linear, then $\tau_{ij}^r = 0$ and there would be no direct effect of the subgrid-scale motions on the filtered motions, and no closure problem.

It is useful to first examine the energetics of the filtered fields. The filtered kinetic energy is

$$\bar{E} = \frac{1}{2}\overline{U_i U_i} \,. \tag{21}$$

On the other hand, the kinetic energy of the filtered motions ($\bar{U}_i$) is

$$E_f = \frac{1}{2}\bar{U}_i\bar{U}_i \text{ (this can be directly computed from an LES).} \tag{22}$$

Note that

$$\bar{E} - E_f = \frac{1}{2}\overline{U_i U_i} - \frac{1}{2}\bar{U}_i\bar{U}_i = \frac{1}{2}\tau_{ii}^R = k_{sgs}$$

from Equation (18). So

$$\bar{E} = E_f + k_{sgs} \,.$$

The dynamic equation for the kinetic energy of the filtered motions E_f can be obtained by multiplying Equation (20) by $\bar{U}_i$ and summing on i. The result is:

$$\frac{\partial}{\partial t}\frac{1}{2}\bar{U}_i^2 + \bar{U}_j\frac{\partial}{\partial x_j}\frac{1}{2}\bar{U}_i^2 = \frac{1}{\rho}\bar{U}_i\frac{\partial}{\partial x_i}\bar{p} + \bar{U}_i\nu\frac{\partial^2}{\partial x_j^2}\bar{U}_i - \bar{U}_i\frac{\partial}{\partial x_j}\tau_{ij}^r \,. \tag{23}$$

However,

$$\bar{U}_i\frac{\partial}{\partial x_i}\bar{p} = \frac{\partial}{\partial x_i}\bar{U}_i\bar{p} \text{ using Equation (13),}$$

$$\bar{U}_i\frac{\partial}{\partial x_j}\tau_{ij}^r = \frac{\partial}{\partial x_j}(\bar{U}_i\tau_{ij}^r) - \tau_{ij}^r\frac{\partial}{\partial x_j}\bar{U}_i \,, \text{ and}$$

$$\bar{U}_i\frac{\partial^2}{\partial x_j^2}\bar{U}_i = \bar{U}_i\frac{\partial}{\partial x_j}\Big(\frac{\partial}{\partial x_j}\bar{U}_i + \frac{\partial}{\partial x_i}\bar{U}_j\Big) = 2\bar{U}_i\frac{\partial}{\partial x_j}\bar{S}_{ij} = 2\frac{\partial}{\partial x_j}(\bar{U}_i\bar{S}_{ij}) - 2\bar{S}_{ij}\bar{S}_{ij} \,;$$

again using Equation (13). Plugging these quantities into Equation (23) gives, finally:

$$\underbrace{\Big(\frac{\partial}{\partial t}+\bar{U}_j\frac{\partial}{\partial x_j}\Big)E_f}_{\substack{\text{rate-of-change}\\ \text{following}\\ \text{filtered motion}}} = \underbrace{\frac{\partial}{\partial x_j}\Big\{-\bar{U}_i\Big(\frac{\bar{p}}{\rho}\delta_{ij}+\tau^r_{ij}+2\nu\bar{S}_{ij}\Big)\Big\}}_{\substack{\text{filtered pressure, sgs,}\\ \text{and viscous transport}}} - \underbrace{2\nu\bar{S}_{ij}\bar{S}_{ij}}_{\substack{\text{dissipation rate of}\\ \text{filtered motions}}} + \underbrace{\tau^r_{ij}\bar{S}_{ij}}_{\substack{\text{loss to sgs}}} \tag{24}$$

The last term on the RHS represents the loss (gain) of energy from the grid-scale motions E_f to (from) the subgrid-scale motions $k_r = \frac{1}{2}U_iU_i - \frac{1}{2}\bar{U}_i\bar{U}_i$ (see Figure 10). In general it is expected that the net transfer is from E_f to k_r, although some 'back-scattering' from the subgrid-scales to the grid-scales is expected to occur.

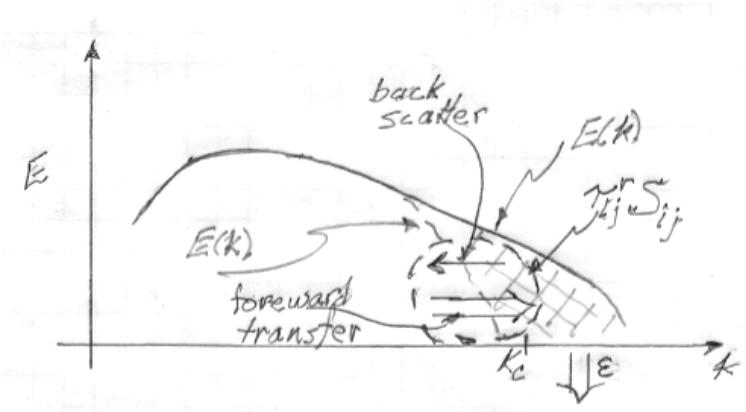

Figure 10: Cartoon of the energy transfer from the filtered (grid-scale) motions to the subgrid-scale motions.

Note that for very high Reynolds number flows, if the filter width Δ is in the inertial range (or is even smaller), then there is very little energy in the subgrid-scale motions, and $\frac{1}{2}\bar{U}_i\bar{U}_1 \approx \frac{1}{2}U_iU_i = E$. If, however, there is appreciable energy in the subgrid-scale motions, then an estimate is needed for the subgrid-scale energy, defined here as the kinetic energy in the unfiltered motions minus the kinetic energy in the filtered (grid-scale) motions, i.e.,

$$k_r = E - \frac{1}{2}\bar{U}_i\bar{U}_i\,. \tag{25}$$

Note that $k_{sgs} \neq k_r$ (see Equation (18)). For homogeneous, isotropic turbulence, the energy spectrum for k_r is (see Problem 13.7, page 570 and Problem 13.10, page 577 of the text):

$$E_r(k) = E(k) - \bar{E}(k) = \big[1 - |\hat{G}(k)|^2\big]E(k)\,, \tag{26}$$

where $E(k)$ is the energy spectrum of the unfiltered motions (the 'true' energy spectrum), and $\hat{G}(k)$ is the Fourier transform of the filter function $G(r)$. Therefore,

$$\langle k_r\rangle = \int_0^\infty \big[1 - |\hat{G}(k)|^2\big]E(k)dk\,. \tag{27}$$

An equation for k_r can be obtained by subtracting the equation for $\frac{1}{2}\bar{U}_i\bar{U}_i$ from that for $\frac{1}{2}U_iU_i$, giving:

$$\begin{aligned}\frac{\partial}{\partial t}k_r + \bar{U}_j\frac{\partial}{\partial x_j}k_r + u'_j\frac{\partial}{\partial x_j}E &= \frac{\partial}{\partial x_j}\Big\{-\frac{1}{\rho}(PU_i - \bar{p}\bar{U}_i)\delta_{ij} + 2\nu(U_iS_{ij} - \bar{U}_i\bar{S}_{ij}) + \bar{U}_i\tau^r_{ij}\Big\} \\ &- 2\nu(S_{ij}S_{ij} - \bar{S}_{ij}\bar{S}_{ij}) - \tau^r_{ij}\bar{S}_{ij}\,. \end{aligned} \tag{28}$$

With appropriate models for τ^r_{ij}, this is sometimes used to predict k_r. There are several LES approaches which use an equation for k_r, somewhat analogous to the use of a k equation in Reynolds-averaged equation modeling. These approaches are mainly in the atmospheric sciences community, where the use of a k_r equation was started by Deardorff, but has continued up to the present time, and in some modeling in the combustion community. In most modeling, however, the assumption is made, sometimes not explicitly, that K_c is in the inertial subrange. Then, based upon Kolmogorov's equilibrium theory, the principal balance in Equation 28 is expected to be:

$$\underbrace{\big\langle -\tau^r_{ij}\hat{S}_{ij}\big\rangle}_{\substack{\text{transfer rate to}\\ \text{subgrid-scales}}} \approx \underbrace{\langle\epsilon\rangle}_{\substack{\text{dissipation rate:}\\ \text{all occurs in}\\ \text{subgrid-scales}}}\,. \tag{29}$$

This implies that all the energy lost by the grid-scale motions is dissipated. Also note that there is the possibility for backscatter, so that $-\tau^r_{ij}\bar{S}_{ij}$ need not be positive everywhere, although it is expected that its average is positive. In fact some modeling attempts to explicitly include the local effects of backscatter.

The use of an equation for k_r should depend, to some extent, on how much kinetic energy is in the subsgrid-scales. If the filter cutoff is in the inertial range, so that there is very little energy in the subgrid-scale motions, and these motions are in approximate equilibrium as assumed by Kolmogorov, then an equation for k_r is probably not needed, and Equation (29) can be assumed. If, however, a significant portion of the energy is in the subgrid-scales, indicating also that the subgrid-scale motions are not in equilibrium and Equation (29) is probably not valid, then it may be important to include a dynamic equation for k_r.

4 Models for τ^r_{ij}

The first model for τ^r_{ij}, introduced by Lilly and based upon a model of Smagorinsky for two-dimensional, atmospheric flows, and still used extensively, is as follows:

$$\tau^r_{ij} = -2\nu_{sgs}\bar{S}_{ij}\,,\ \bar{S}_{ij} = \frac{1}{2}\Big(\frac{\partial}{\partial x_j}\bar{U}_i + \frac{\partial}{\partial x_i}\bar{U}_j\Big)\,, \tag{30}$$

where the subgrid-scale viscosity is giving by

$$\begin{aligned}\nu_{sgs} &= \ell_s^2\bar{\mathcal{S}} \text{ (see the mixing length model, Equation 10.19, page 367 in the text)}\\ \ell_s &= c_s\Delta \text{ with } \Delta \text{ the filter width}\\ \bar{\mathcal{S}} &= (2\bar{S}_{ij}\bar{S}_{ij})^{\frac{1}{2}} \text{ the magnitude of the grid-scale strain rate}\end{aligned}$$

and c_s is the Smagorinsky coefficient. The analogy with the turbulence viscosity modeling of the Reynolds stress is clear. Here there is no need for an additional length scale, as is needed in Reynolds averaged equations modeling, as a length scale, Δ, is already provided by the fiiltering.

Note that the rate of energy transferred from the grid-scale motions to the subgrid-scale motions is

$$-\tau_{ij}^r \frac{\partial}{\partial x_j}\bar{U}_i = +2\nu_{sgs}\bar{S}_{ij}\frac{\partial}{\partial x_j}\bar{U}_i = 2\nu_{sgs}\bar{S}_{ij}\bar{S}_{ij} = \nu_{sgs}\bar{\mathcal{S}}^2 > 0\,,$$

as $\nu_{sgs} > 0$ in the original model. Therefore, for this model, the transfer is always from the grid-scale to the subgrid-scale motions. There is no backscatter.

Following Lilly, the constant in Smagorinsky's model can be estimated, assuming high Reynolds number and that the cutoff wave number K_c is in the initial range. In that case, assuming homogeneous isotropic turbulence, at least for the inertial range,

$$\langle\bar{\mathcal{S}}^2\rangle = 2\langle\bar{S}_{ij}\bar{S}_{ij}\rangle = 2\int_0^\infty k^2\bar{E}(k)dk \approx 2\int_0^\infty k^2|\hat{G})k)|^2 C\langle\epsilon\rangle^{2/3}k^{-5/3}dk\,,$$

with $E(k) = C\langle\epsilon\rangle^{2/3}k^{-5/3}$ in the inertial range, and C Kolmogorov's constant. So

$$\langle\bar{\mathcal{S}}^2\rangle \approx a_f C\langle\epsilon\rangle^{2/3}\Delta^{-4/3}\,,$$

with the constant a_f given by Equation (11), assuming that $\hat{G}(k)$ is a function of $k\Delta$. Solving for $\langle\epsilon\rangle$ gives

$$\langle\epsilon\rangle = (a_f C)^{-3/2}\Delta^2\langle\bar{\mathcal{S}}^2\rangle^{3/2}\,.$$

Assuming that the subgrid-scale motions are in equilibrium, so that Equation (29), then

$$\langle\epsilon\rangle \approx -\langle\tau_{ij}^r\bar{S}_{ij}\rangle = +\langle 2\nu_{sgs}\bar{S}_{ij}\bar{S}_{ij}\rangle = \ell_s^2\langle\bar{\mathcal{S}}^3\rangle = c_s^2\Delta^2\langle\bar{\mathcal{S}}^3\rangle\,.$$

Comparing the previous two equations gives:

$$(a_f C)^{-3/2}\Delta^2\langle\bar{\mathcal{S}}^2\rangle^{3/2} \approx c_s^2\Delta^2\langle\bar{\mathcal{S}}^3\rangle\,.$$

Solving this for c_s gives

$$c_s \approx \frac{1}{(a_f C)^{3/4}}\frac{\langle\bar{\mathcal{S}}^2\rangle^{3/4}}{\langle\bar{\mathcal{S}}^3\rangle}\,.$$

For the sharp spectral filter, it was found that $a_f \approx 6.9$. Furthermore, from laboratory data, $C \approx 1.5$. Finally, assuming that $\langle\bar{\mathcal{S}}^2\rangle^{3/4} \approx \langle\bar{\mathcal{S}}^3\rangle^{1/2}$, then

$$c_s \approx \frac{1}{(1.5\cdot\frac{3}{2}\pi^{4/3})^{3/4}} = \frac{1}{(1.5\cdot\frac{3}{2})^{3/4}}\frac{1}{\pi} \approx 0.17\,,$$

that is, $c_s \approx 0.17$. This is the estimate originally made by Lilly. We will find later from comparisons of simulation results with data that this is a little off. The value of c_s is usually recommended as about 0.1. The main point of this analysis, though, is to show that c_s can be theoretically estimated. We will see later that it can be estimated 'on the fly' during a simulation.

4.1 Limiting behavior of Smagorinsky's model

It is often useful to test a model by examining its limiting behavior, which can give insights into the strengths and weaknesses of the model. There are at least two cases for which Smagorinsky's model should be consistent.

- Consider the limit as $\dfrac{\Delta}{\eta} \to 0$. In this case the LES should reduce to a DNS, i.e., $\tau_{ij}^r \to 0$. Here $\eta = (\nu^3/\epsilon)^{1/4}$ is the Kolmogorov scale, the characteristic scale for the dissipation range, and 'below' which there is no relevant energy.

- For laminar flows, e.g., in transition to turbuence, $\tau_{ij}^r \to 0$, since there should be no subgrid-scale stresses; the motion is not turbulent. It is, or it can be, non-linear, but it is not broad-banded (or it would be turbulent).

Consider first the limit as $(\Delta/\eta) \to 0$. With Smagorinsky's model, the filtered momentum equation is:

$$\frac{\partial}{\partial t}\bar{U}_i + \bar{U}_j\frac{\partial}{\partial x_j}\bar{U}_i = -\frac{1}{\rho}\frac{\partial}{\partial x_i}\bar{p} + \frac{\partial}{\partial x_j}\Big\{(\nu+\nu_{sgs})\bar{S}_{ij}\Big\}\,,$$

with $\nu_{sgs} = \ell_s^2\bar{\mathcal{S}}$, $\ell_s = c_s\Delta$. Of interest is to compare the ratio ν_{sgs}/ν as $\Delta/\eta \to 0$. To estimate ν_{sgs} we use

$$\langle\nu_{sgs}^2\rangle^{1/2} = \langle\ell_s^4\bar{\mathcal{S}}\bar{\mathcal{S}}\rangle^{1/2} \to \ell_s^2\langle S_{ij}S_{ij}\rangle^{1/2} = \ell_s^2\Big(\frac{\epsilon}{2\nu}\Big)^{1/2} \text{ as } \frac{\Delta}{\eta} \to 0$$

since $\bar{S}_{ij} \to S_{ij}$ and $\epsilon = 2\nu\langle S_{ij}S_{ij}\rangle$. So

$$\frac{\langle\nu_{sgs}^2\rangle^{1/2}}{\nu} \to \frac{1}{\sqrt{2}}\ell_s^2\Big(\frac{\epsilon}{\nu^3}\Big)^{1/2} = \frac{c_s^2}{\sqrt{2}}\frac{\Delta^2}{\eta^2} \to 0 \text{ as } \frac{\Delta}{\eta} \to 0\,.$$

Therefore, according to Smagorinsky's model, the residual stress model $\tau_{ij}^r = -2\nu_{sgs}\bar{S}_{ij} \to 0$, compared to the viscous stress $\tau_{ij}^{viscous} = \nu S_{ij}$, as $\Delta/\eta \to 0$, an important property of the model.

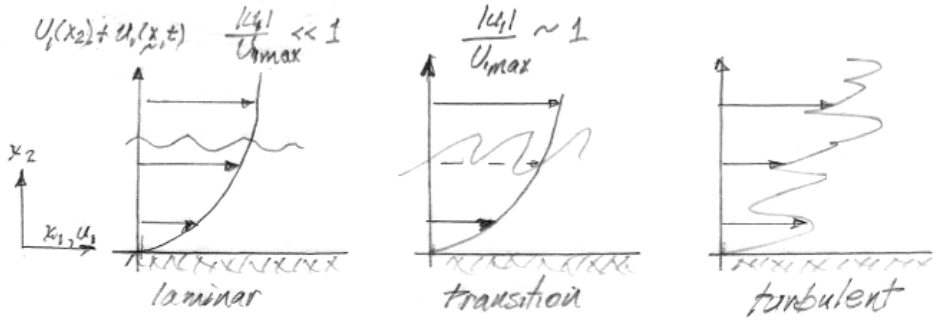

Figure 11: Cartoon of a simulation of the transition to turbulence.

Second, consider laminar flows. It is sometimes important to compute the transition to turbulence, the flow going from laminar to turbulent flow, as sketched in Figure 11. The spectral bandwidth of a laminar flow tends to be fairly narrow, which could be considered to be the definition of a flow which is not turbulent (see Figure 12). Now the estimate of ν_{sgs} is much different for this case. With ℓ_I the scale of the instability, i.e., the energy-containing scale for a transition problem, then

$$\langle\nu_{sgs}^2\rangle^{1/2} = \ell_s^2\langle\bar{S}_{ij}\bar{S}_{ij}\rangle^{1/2} \sim \ell_s^2\frac{\mathcal{U}}{\ell_I} = c_s^2\Delta^2\frac{\mathcal{U}}{\ell_I} = c_s^2\mathcal{U}\ell_I\frac{\Delta^2}{\ell_I^2}\,,$$

where $\mathcal{U}$ is a characteristic velocity of the instability. So

$$\frac{\langle\nu_{sgs}^2\rangle^{1/2}}{\nu} \sim c_s^2\frac{\mathcal{U}\ell_I}{\nu}\frac{\Delta^2}{\ell_I^2} = c_s^2 Re\frac{\Delta^2}{\ell_I^2} \text{ with } Re = \frac{\mathcal{U}\ell_I}{\nu}\,.$$

There are 2 possible cases here.

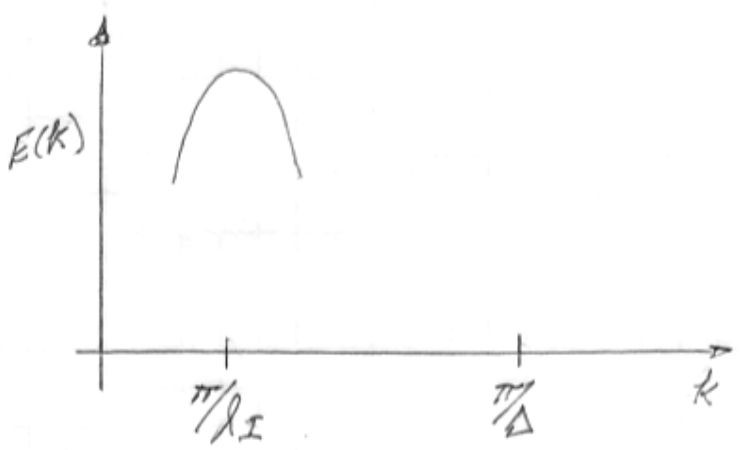

Figure 12: Cartoon of the energy spectrum for a laminar, perturbed flow.

- If $\Delta/\ell_I \to 0$, there would be a well-resolved direct numerical simulation of the transition to turbulence.
- For finite Δ/ℓ_I, usually Re is large enough that $c_s^2 Re\left(\frac{\Delta}{\ell_I}\right)^2$ is much greater than 1. In this case, the model 'acts' as if the flow were turbulent. There is nothing in the modeling to say that the flow is not turbulent. There results an apparent viscosity which is much higher than the fluid viscosity. This results in either

  1. slowing the growth rate of the instability, or
  2. totally eliminating the instability,

  since the effective Reynolds number, based upon ν_{sgs} is smaller than the true Reynolds number, i.e.,

$$\frac{\mathcal{U}\ell_I}{\nu_{sgs}} < \frac{\mathcal{U}\ell_I}{\nu}\,.$$

  This is a major flaw in the model, leading to erroneous transition simulations. We will see that this flaw is, to some extent, eliminated by dynamic modeling.

5 Dynamic modeling

Dynamic modeling is one of the better ideas that has come along since the inception of large-eddy simulations. Here it will be discussed with application to Smagorinsky's model, but it can also be applied to other subgrid-scale models. It starts with the idea that, in considering spectral energy transfer, most interactions are thought to be local in wave number space. This has been verified, to some extent, by direct numerical simulations in which spectral energy transfer can be directly computed. There are some interactions, however, which are clearly non-local, such as wave-wave interactions; these are not relevant in the present discussions, however. Considering the interactions as local, then the major influence of the subgrid-scale motions on the grid-scale motions occurs near the cutoff (see Figure 13).

A problem with Smagorinsky's model is that it weights the entire energy-containing range too much. This is probably a major reason why Smagorinsky's model does not work well for

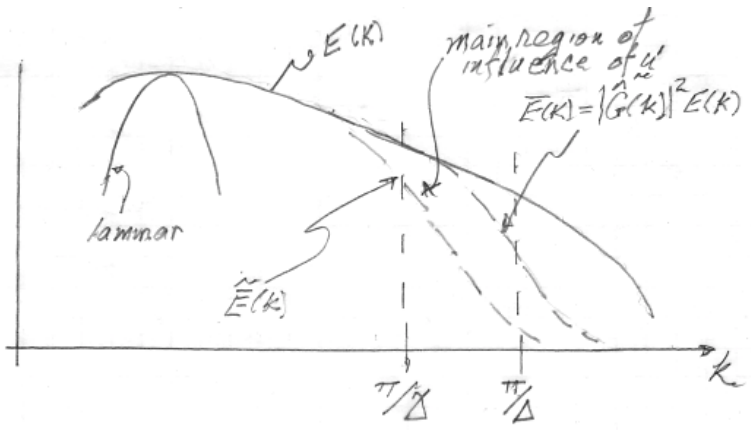

Figure 13: Cartoon depicting the region in wave number space where the influence of the subgrid-scale on the grid-scale motions is greatest.

transitioning flows. A method to isolate the scales of motion next to the filter cutoff is by using a second filter, with the filter size $\tilde{\Delta} > \Delta$ (often $\tilde{\Delta} = 2\Delta$ is chosen). So we define a second filter as:

$$\tilde{\bar{U}} = \int \tilde{G}(\mathbf{r}, \mathbf{x}) \bar{U}(\mathbf{x} - \mathbf{r}) d\mathbf{r} \,, \tag{31}$$

assuming, for now, a homogeneous (independent of $\mathbf{x}$), isotropic (depending only on $|\mathbf{r}|$) filter. Note that we can write:

$$\mathbf{U} = \bar{\mathbf{U}} + \mathbf{u}' = \underbrace{\tilde{\bar{\mathbf{U}}}}_{\substack{\text{double} \\ \text{filtered}}} + \underbrace{(\bar{\mathbf{U}} - \tilde{\bar{\mathbf{U}}})}_{\substack{\text{scales} \\ \text{near cutoff}}} + \underbrace{\mathbf{u}'}_{\substack{\text{original} \\ \text{residual}}} \,. \tag{32}$$

We next consider the implications of this second filtering. If the momentum equation is filtered twice, first with $\bar{(\cdot)}$ and then with $\tilde{(\cdot)}$, with corresponding filter widths Δ and $\tilde{\Delta} > \Delta$, the result is (with G and $\tilde{G}$ independent of $\mathbf{x}$):

$$\frac{\partial}{\partial t}\tilde{\bar{U}}_i + \frac{\partial}{\partial x_j}\widetilde{\overline{U_i U_j}} = -\frac{1}{\rho}\frac{\partial}{\partial x_i}\tilde{\bar{p}} + \nu \frac{\partial^2}{\partial x_j^2}\tilde{\bar{U}}_i \,. \tag{33}$$

It is then natural to define the subgrid-scale (residual) stress due to double filtering as:

$$T_{ij} = \widetilde{\overline{U_i U_j}} - \tilde{\bar{U}}_i \tilde{\bar{U}}_j \,, \text{ giving in Equation (33),} \tag{34}$$

$$\frac{\partial}{\partial t}\tilde{\bar{U}}_i + \tilde{\bar{U}}_j \frac{\partial}{\partial x_j}\tilde{\bar{U}}_i = -\frac{1}{\rho}\frac{\partial}{\partial x_i}\tilde{\bar{p}} + \nu \frac{\partial^2}{\partial x_j^2}\tilde{\bar{U}}_i - \frac{\partial}{\partial x_j} T_{ij} \,. \tag{35}$$

The problem now is how to determine T_{ij}. Note that:

$$\mathcal{L}_{ij} \equiv T_{ij} - \widetilde{\tau_{ij}^R} = [\widetilde{\overline{U_i U_j}} - \tilde{\bar{U}}_i \tilde{\bar{U}}_j] - [\widetilde{\overline{U_i U_j}} - \widetilde{\bar{U}_i \bar{U}_j}] = \widetilde{\bar{U}_i \bar{U}_j} - \tilde{\bar{U}}_i \tilde{\bar{U}}_j \,, \tag{36}$$

called Germano's identity. Note that the right-hand side of Equation (36) can be directly computed, given $\bar{U}_i$. The left-hand side, however, requires some modeling. Also note that the right-hand side is in the form of a subgrid-scale stress with respect to the second filter, given $\bar{U}_i$.

What does this imply about Smagorinsky's model? His model for τ_{ij}^R is (see Equation (30) and the following):

$$\tau_{ij}^r = \tau_{ij}^R - \frac{1}{3}\tau_{kk}^R\delta_{ij} = -2\hat{c}_s\Delta^2\bar{\mathcal{S}}\bar{S}_{ij}\,,\ \hat{c}_s = c_s^2\,.$$

Assuming that the Smagorinsky model also holds for T_{ij}, and with the same constant $\hat{c}_s$, then the anisotropic, deviatoric part of T_{ij} is given as

$$T_{ij}^d = T_{ij} - \frac{1}{3}T_{kk}\delta_{ij} = -2\hat{c}_s\tilde{\Delta}^2\tilde{\bar{\mathcal{S}}}\tilde{\bar{S}}_{ij}\,,$$

which is, of course, a major assumption. Therefore, for the anisotropic, deviatoric part of Germano's identity, the model for the left-hand side of Equation (36) is:

$$T_{ij}^d - \widetilde{\tau_{ij}^r} = \hat{c}_s\Big\{2\Delta^2\widetilde{\bar{\mathcal{S}}\bar{S}_{ij}} - 2\tilde{\Delta}^2\tilde{\bar{\mathcal{S}}}\tilde{\bar{S}}_{ij}\Big\} = \hat{c}_s\mathcal{M}_{ij}\,,\ \text{say.} \tag{37}$$

Note that:

- $\mathcal{M}_{ij}$ is computable, given $\bar{U}_i$, and
- it was assumed that the constant $\hat{c}_s$ was unaffected by the filtering of τ_{ij}^r.

Furthermore, the anisotropic, deviatoric part of $\mathcal{L}_{ij}$ is:

$$\mathcal{L}_{ij}^d = \mathcal{L}_{ij} - \frac{1}{3}\mathcal{L}_{kk}\delta_{ij} = \widetilde{\bar{U}_i\bar{U}_j} - \tilde{\bar{U}}_i\tilde{\bar{U}}_j - \frac{1}{3}\Big(\widetilde{\bar{U}_k^2} - \tilde{\bar{U}}_k^2\Big)\delta_{ij}\,. \tag{38}$$

This is also directly computable given $\bar{U}_i$. Therefore, the anisotropic, deviatoric part of Equation (36), where the left-hand side is now modeled as Equation (37) and the right-hand side is given by Equation (38):

$$\mathcal{L}_{ij}^d = \hat{c}_s\mathcal{M}_{ij}\,. \tag{39}$$

Since both $\mathcal{L}_{ij}^d$ and $\mathcal{M}_{ij}$ in Equation (39) can be computed, given $\bar{U}_i$, then this equation can be used to compute $\hat{c}_s$ (and hence c_s) locally in space and time.

There are at least two problems with this argument.

- Both $\mathcal{L}_{ij}^d$ and $\mathcal{M}_{ij}$ are symmetric tensors (matrices). Therefore there are actually 6 different equations for $\hat{c}_s$, with no guarantee that each equation will yield the same value for $\hat{c}_s$. If fact they may give very different values.
- Is is assumed that the $\hat{c}_s$'s are not affected by the filtering when τ_{ij}^r is filtered. This has been demonstrated by direct numerical simulations to be in error.

Lilly suggested that, instead of using Equation (39) to obtain the different $\hat{c}_s$'s, use the value of $\hat{c}_s$'s that minimizes the mean square error in Equation (39) in the following sense. Consider the error in the estimation to be E_r. Then

$$E_r = \Big(\hat{c}_s\mathcal{M}_{ij} - \mathcal{L}_{ij}^d\Big)\Big(\hat{c}_s\mathcal{M}_{ij} - \mathcal{L}_{ij}^d\Big)\,,$$

summing in i, j. So to minimize the error,

$$\frac{\partial E_r}{\partial\hat{c}_s} = 2\mathcal{M}_{ij}\Big(\hat{c}_s\mathcal{M}_{ij} - \mathcal{L}_{ij}^d\Big) = 2\Big\{\hat{c}_s\mathcal{M}_{ij}\mathcal{M}_{ij} - \mathcal{M}_{ij}\mathcal{L}_{ij}^d\Big\} = 0\,,\ \text{or}$$

$$\hat{c}_s = \frac{\mathcal{M}_{ij}\mathcal{L}_{ij}^d}{\mathcal{M}_{k\ell}\mathcal{M}_{k\ell}}\,. \tag{40}$$

Note the following.

- Equation (40) can be computed pointwise to determine $\hat{c}_s$.
- $\dfrac{\partial^2}{\partial \hat{c}_s^2} E_r = 2\mathcal{M}_{ij}\mathcal{M}_{ij} > 0$ (all components of $\mathcal{M}_{ij}$ are real), so that E_r is a minimum for $\hat{c}_s$ satisfying Equation (40).

Note that it is possible, and in fact usually the case, that some values of $\hat{c}_s$ are negative. Some people have argued that this naturally represents 'backscatter', i.e., energy transfer from the residual motions to the grid-scale motions (negative sgs viscosity), i.e., locally positive values of $\tau_{ij}^r \bar{S}_{ij}$ in the equation for $\dfrac{1}{2}\bar{U}_i^2$, Equation (24). It is known from direct numerical simulations that 'backscatter' can occur somewhat locally in space and time, although longer-term and/or larger-scale averages always show a net transfer from the grid-scale to the subgrid-scale motions.

Comparing modeling results with direct numerical simulation results, *a priori* tests indicate that backscatter does not correlate with negative values of $\hat{c}_s$. Furthermore, large-eddy simulation using $\hat{c}_s$ directly computed from Equation (40) are found to be numerically unstable, as small regions of negative $\hat{c}_s$ can lead to fast, unstable growth of $\bar{U}_i$. Therefore, to eliminate this instability, $\hat{c}_s$ is usually averaged in one of the following ways:

- average $\hat{c}_s$ in directions of statistical homogeneity;
- average over 'local' regions;
- average over Lagrangian trajectories.

5.1 Methods to test models

There are at least two ways to test models using high resolution laboratory data or direct numerical simulation data.

- *a posteriori* – (after the fact). This is the usual way to test models. Run the model and then compare the model output and predictions with the laboratory and direct numerical simulation data.
- *a priori* – no simulation needs to be run. Use the high resolution laboratory and direct numerical simulation data to test specific components of the model. For example,

$$\tau_{ij}^r = \overline{U_i U_j} - \bar{U}_i\bar{U}_j - \frac{2}{3}(\frac{1}{2}\overline{U_k U_k} - \frac{1}{2}\bar{U}_k\bar{U}_k)\delta_{ij} \overset{?}{=} -2\nu_{sgs}\bar{S}_{ij} \text{ with } \nu_{sgs} = \ell_s^2\bar{\mathcal{S}}\,,\ \ell_s = c_s\Delta\,.$$

  Given U_i, both sides of the equation can be directly computed to determine the validity of the model.

5.2 Example of *a posteriori* testing

In dynamic modeling, one must deal with the fact that, in the original formulation of the model, the constant $\hat{c}_s$ does not pass through the second filtering operator. This can be directly treated by solving a much more difficult numerical problem (Ghosal et al., 1995), by what is called the 'dynamic localization model'. A simpler approach to achieve the same goal was proposed and implemented by Piomelli and Liu (1995; a copy is on the course website). They performed large-eddy simulations of a rotating channel flow, with the configuration show in Figure 14. The mean flow is in the x_1 direction, with the x_2 direction normal to the boundaries, and the rotation vector

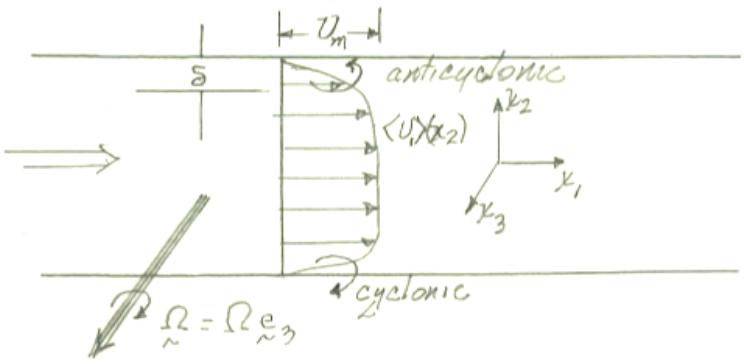

Figure 14: Sketch of rotating turbulent channel flow. System rotation vector is in the x_3 direction. Top boundary layer has vorticity (rotation) in the opposite direction to the system rotation (anti-cyclonic), while the bottom boundary layer has vorticity in the same direction as system rotation (cyclonic).

$\mathbf{\Omega} = \Omega \mathbf{e}_3$ in the x_3 direction. Note that this type of flow has several applications, e.g., the flow between turbine blades, and geophysical flows on intermediate scales.

To treat the fact that $\hat{c}_s$ could become negative and destabilize the flow, and since the flow is statistically homogeneous in each horizontal plane, $\hat{c}_s$ was averaged in each horizontal plane so that it was always positive, although not constant. The no-slip condition was applied at the boundaries. This is an important, difficult test case for models because of the behavior of the flow near the two boundaries. Define the Rossby number (or inverse rotation number) as:

$$Ro = \frac{U_m}{\Omega \delta} \,,$$

with U_m a peak mean velocity, and δ a boundary layer thickness at each boundary. It is known that, if the Rossby number is of order 1, then

- near the lower boundary, where the system rotation is in the same direction as the mean boundary layer rotation (vorticity), which is sometimes called cyclonic, the effect of rotation is to stabilize the flow, whereas
- near the upper boundary, where the system rotation is in the opposite direction to the mean boundary layer rotation (anti-cyclonic), the effect of rotation is to destabilize the flow.

The method to evaluate the coefficient $\hat{c}_s$, called 'approximate localization', is as follows. To simplify the notation, write

$$\tau_{ij}^r = -2\hat{c}_s \Delta^2 \bar{\mathcal{S}} \bar{S}_{ij} \equiv -2\hat{c}_s \beta_{ij} \,, \text{ and}$$

$$T_{ij}^d = -2\hat{c}_s \tilde{\Delta}^2 \tilde{\bar{\mathcal{S}}} \tilde{\bar{S}}_{ij} = -2\hat{c}_s \alpha_{ij} \,. \text{ Then}$$

$$\mathcal{L}_{ij}^m = T_{ij}^d - \widetilde{\tau_{ij}^r} = -2\hat{c}_s \alpha_{ij} + 2\widetilde{\hat{c}_s \beta_{ij}} \text{ (model } \mathcal{S}),$$

so using Germano's identity, Equation (36), then

$$\mathcal{L}_{ij}^d = -2\hat{c}_s \alpha_{ij} + 2\widetilde{\hat{c}_s \beta_{ij}} \,,$$

where we would like to solve for c_s. Unfortunately $\hat{c}_s$ does not appear explicitly, but is inside the filtering operator, resulting in an integral equation for $\hat{c}_s$, which cannot be easily solved. If we have an estimate for $\hat{c}_s$, say c_s^*, then we could solve for $\hat{c}_s$ by minimizing

$$E_r = \left(\mathcal{L}_{ij}^d + 2\hat{c}_s\alpha_{ij} - 2\widetilde{c_s^*\beta_{ij}}\right)\left(\mathcal{L}_{ij}^d + 2\hat{c}_s\alpha_{ij} - 2\widetilde{c_s^*\beta_{ij}}\right), \text{ or}$$

$$\frac{\partial E_r}{\partial \hat{c}_s} = 4\alpha_{ij}\left(\mathcal{L}_{ij}^d + 2\hat{c}_s\alpha_{ij} - 2\widetilde{c_s^*\beta_{ij}}\right) = 0\,, \text{ or}$$

$$2\hat{c}_s\alpha_{ij}\alpha_{ij} = 2\widetilde{c_s^*\beta ij} - \alpha_{ij}\mathcal{L}_{ij}^d\,, \text{ or, finally}$$

$$\hat{c}_s = \frac{2\widetilde{c_s^*\beta_{ij}}\alpha_{ij} - \alpha_{ij}\mathcal{L}_{ij}^d}{2\alpha_{ij}\alpha_{ij}}\,. \tag{41}$$

The problem now is to get a good estimate for c_s^*. Piomelli and Liu obtained c_s^* from its previous values in time $(n-1)$, either as:

- $c_s^* = \hat{c}_s^{n-1}$ (0^{th} order), or
- $c_s^* = \hat{c}_s^{n-1} + \left.\frac{\partial \hat{c}_s}{\partial t}\right|_{n-1}\Delta t$ with $\left.\frac{\partial \hat{c}_s}{\partial t}\right|_{n-1} = \frac{\hat{c}_s^{n-1} - \hat{c}_s^{n-1}}{t_{n-2} - t_{n-1}}$ (1^{st} order), or
- iteratively, by plugging $\hat{c}_s|_{\text{new}}$ into Equation (41) for c_s^*, and recomputing it.

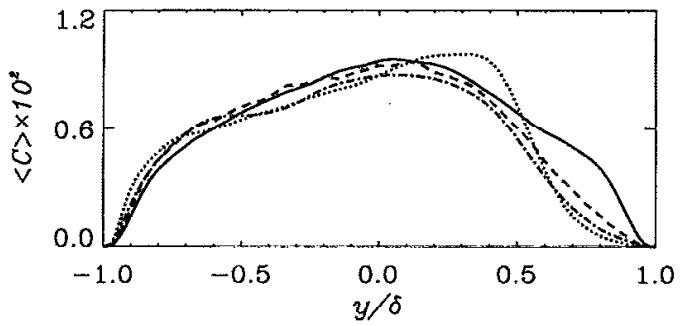

Figure 15: Horizontally-averaged $\hat{c}_s$ as a function of y (x_2).

Figure 15 contains plots, for different values of the Rossby number, of the horizontally-averaged $\hat{c}_s$ as a function of y (x_2) taken from a typical simulation of Piomelli and Liu. The dependence of the coefficient on space is very clear and the use of a constant value of $\hat{c}_s$ would appear to be problematic. Figure 16 contains plots of the mean velocity taken from a particular case. Figure 16(a) gives the entire profile, with the cyclonic side at $y/\delta = x_2/\delta = 1.0$, while $y/\delta = -1.0$ is the cyclonic side. In Figures 16(b) and 16(c) is given the profiles in wall units (the distance from the boundary divided by the viscous length ν/u_* where u_* is the wall shear stress) on the cyclonic and anti-cyclonic sides, respectively.

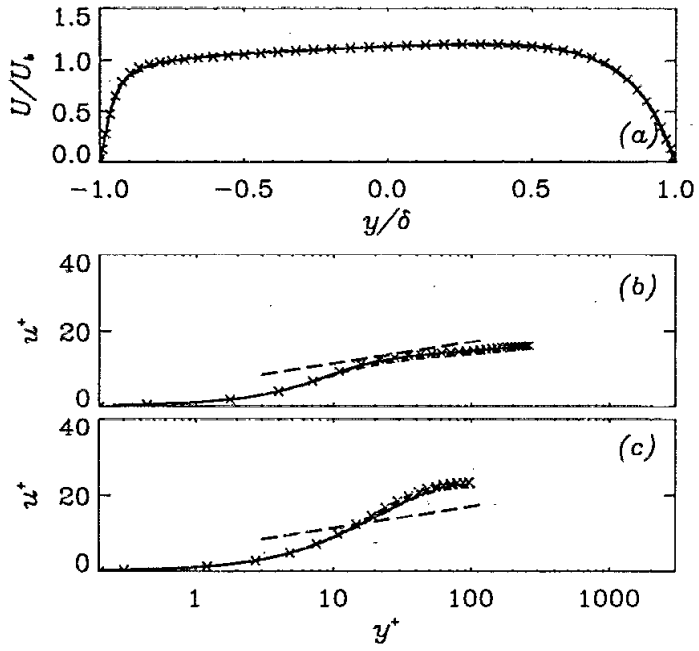

Figure 16: (a) Mean velocity as a function of y/δ; (b) mean velocity in wall units for the anti-cyclonic side; (c) mean velocity in wall units for the cyclonic side.

6 Scale-similarity models

The scale similarity models are another attempt to emphasize information near the filter cutoff in modeling the effects of the residual scales. In the original version of the scale-similarity models, it was argued that, since

$$\tau_{ij}^R = \overline{U_i U_j} - \bar{U}_i \bar{U}_j \,,$$

the result of filtering U_i, then an approximation to τ_{ij}^R can be obtained by filtering $\bar{U}_i$ instead, i.e., (see Bardina et al., 1980),

$$\mathcal{L}_{ij}^o = \overline{\bar{U}_i \bar{U}_j} - \bar{\bar{U}}_i \bar{\bar{U}}_j \,. \tag{42}$$

The result is called a "Leonard stress", although this term is used loosely. Note that $\mathcal{L}_{ij}^o$ can be computed directly from $\bar{U}_i$. The simplest version of this model is then of the form,

$$\tau_{ij}^R = c_m \Big(\overline{\bar{U}_i \bar{U}_j} - \bar{\bar{U}}_i \bar{\bar{U}}_j \Big) \,,$$

where the constant c_m is of order 1, and can be computed dynamically.

A variation of this is to define a second filter, with filter width $\tilde{\Delta} > \Delta$ and denoted by $\tilde{(\cdot)}$ as above. The model is then

$$\tau_{ij}^R = \tilde{c}_m \Big(\widetilde{\bar{U}_i \bar{U}_j} - \tilde{\bar{U}}_i \tilde{\bar{U}}_j \Big) \,.$$

It is called 'scale-similarity' because it is argued heuristically that the two filtering operations should do about the same thing if the spectral properties are the same at π/Δ and $\pi/\tilde{\Delta}$ (see Figure 17). Note that the scale similarity model gives very good correlation with the 'exact' residual stress (computed using data from very high resolution direct numerical simulations or laboratory

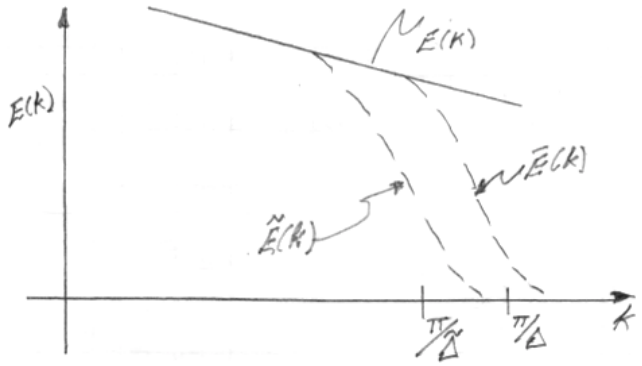

Figure 17: Cartoon to explain the idea of scale similarity.

experiments), as high as 80% (see Figure 18, discussed below), which compares the scale similarity model with the 'exact' residual stress).

Unfortunately, in homogeneous decay studies where, for example, accurately modeling of the dissipation rate is of paramount importance, the scale-similarity model does not 'dissipate' enough energy. Therefore, a 'mixed' model has been suggested. The original motivation for it is as follows. With the decomposition $U_i = \bar{U}_i + u_i'$, then

$$\begin{aligned} \tau_{ij}^R &= \overline{U_i U_j} - \bar{U}_i \bar{U}_j = \overline{(\bar{U}_i + u_i')(\bar{U}_j + u_j')} - \bar{U}_i \bar{U}_j \\ &= \underbrace{\overline{\bar{U}_i \bar{U}_j} - \bar{U}_i \bar{U}_j}_{\substack{\text{original Leonard} \\ \text{stress } \mathcal{L}_{ij}}} + \underbrace{\overline{\bar{U}_i u_j'} + \overline{\bar{U}_j u_i'}}_{\text{cross stresses}} - \underbrace{\overline{u_i' u_j'}}_{\substack{\text{sgs Reynolds} \\ \text{stress}}} . \end{aligned} \tag{43}$$

The original mixed model retains the first term in Equation (43) as a 'scale-similarity' model, and models the last two terms together with Smagorinsky's model. The latter part of the model supplies the adequate dissipation rate. There is a theoretic issue with this, that the original Leonard stress is not Galilean invariant (Galilean invariance will be discussed in the next section). A modified version of Equation (43) that was suggested by Germano (see the text, Equation 13.99, 13.100, page 583) is Galilean invariant, using the Leonard stress in Equation (42). A doubly-filtered model is now preferred, i.e.,

$$\tilde{\mathcal{L}}_{ij} = \widetilde{\bar{U}_i \bar{U}_j} - \tilde{\bar{U}}_i \tilde{\bar{U}}_j \, .$$

The mixed model is then

$$\tau_{ij}^r = \hat{c}_m \Big(\tilde{\mathcal{L}}_{ij} - \frac{1}{3} \tilde{\mathcal{L}}_{kk} \delta_{ij} \Big) - 2 \hat{c}_s \Delta^2 \bar{\mathcal{S}} \bar{S}_{ij} \, . \tag{44}$$

The two coefficients, $\hat{c}_m$ and $\hat{c}_s$, can be determined dynamically. This model gives the best results of various tests. For example, in Figure 18 is compared the residual stress computed directly from laboratory data, from Smagorinsky's model, and from the mixed model. There is little visual correlation between the laboratory results and Smagorinsky's model. There is, however, noticeable agreement between the laboratory data and the mixed model.

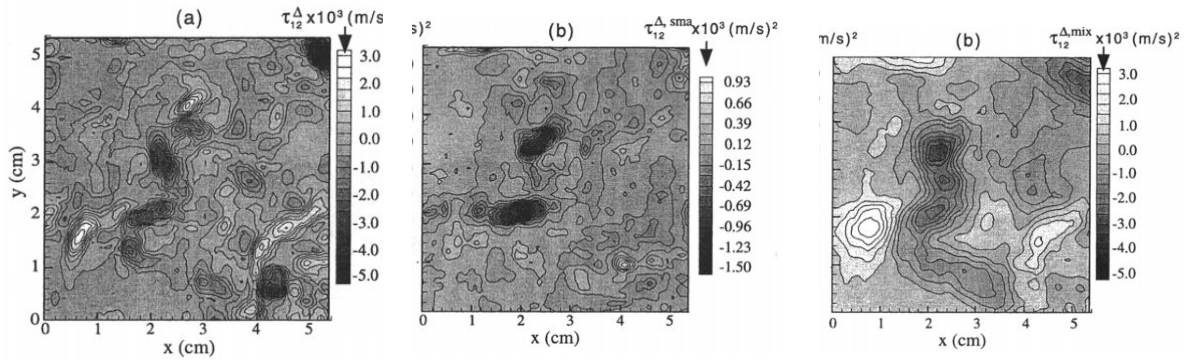

(a) laboratory data (b) Smagorinsky model (c) mixed model

Figure 18: Comparison of the residual stress computed from (a) high-resolution laboratory data; (b) Smagorinsky's model; (c) the mixed model. Taken from Katz et al., 2000.

6.1 Galilean Invariance

It is expected that, with the residual stress $\tau_{ij}^r = \overline{U_i U_j} - \bar{U}_i \bar{U}_j$ defined in an inertial reference frame, then the same stress should be obtained in another reference frame moving at a constant velocity $-\mathbf{V}$ with respect to the first frame. In the new reference frame, with the velocity $W_i = U_i + V_i$, then the residual stress is:

$$\begin{aligned}
\overline{W_i W_j} - \bar{W}_i \bar{W}_j &= \overline{(U_i + V_i)(U_j + V_j)} - \overline{(U_i + V_i)}\,\overline{(U_j + V_j)} \\
&= \overline{U_i U_j} + \underbrace{\bar{U}_i V_j + V_i \bar{U}_j + V_i V_j}_{\text{cancel out}} - (\bar{U}_i \bar{U}_j + \underbrace{\bar{U}_i V_j + V_i \bar{U}_j + V_i V_j}_{\text{cancel out}}) \\
&= \overline{U_i U_j} - \bar{U}_i \bar{U}_j \,,
\end{aligned}$$

i.e., the residual stress is Galilean invariant. This implies that any model for the residual stress should also be Galilean invariant.

On the other hand, the original Leonard stress is not Galilean invariant, as can be seen as follows with $W_i = U_i + V_i$.

$$\begin{aligned}
\overline{\bar{W}_i \bar{W}_j} - \bar{W}_i \bar{W}_j &= \overline{(\bar{U}_i + V_i)(\bar{U}_j + V_j)} - (\bar{U}_i + V_i)(\bar{U}_j + V_j) \\
&= \overline{\bar{U}_i \bar{U}_j} + \bar{\bar{U}}_i V_j + \bar{\bar{U}}_j V_i + \underbrace{V_i V_j}_{\text{cancel}} - (\bar{U}_i \bar{U}_j + \bar{U}_i V_j + \bar{U}_j V_i + \underbrace{V_i V_j}_{\text{cancel}}) \\
&= \underbrace{\overline{\bar{U}_i \bar{U}_j} - \bar{U}_i \bar{U}_j}_{\text{original form}} + (\bar{\bar{U}}_i - \bar{U}_i) V_j + (\bar{\bar{U}}_j - \bar{U}_j) V_i \,.
\end{aligned}$$

This is not Galilean invariant except for filters satisfying $\bar{\bar{U}}_i = \bar{U}_i$, indicating that it does not have the expected consistency properties in general.

On the other hand, the two double filtered quantities, $\widetilde{\bar{U}_i \bar{U}_j} - \tilde{\bar{U}}_i \tilde{\bar{U}}_j$ and $\overline{\bar{U}_i \bar{U}_j} - \bar{\bar{U}}_i \bar{\bar{U}}_j$ are Galilean invariant, as can be easily shown.

7 Transport equations for residual quantities

Transport equations for residual quantities are used in several areas of research, for example, in some combustion modeling, in the code Fluent, and in modeling of the atmospheric boundary layer.

When Deardorff was performing his large-eddy simulations of turbulent channel flow and then atmospheric boundary layers, there was a lot of activity in the turbulence community in RANS with both k-ϵ and Reynolds stress transport modeling. So he implemented both of these in his large-eddy simulations, going beyond the Smagorinsky model. In particular, he developed

- a transport equation for the residual kinetic energy, k_r, and
- transport equations for the residual stresses.

Note that no addition equation, for example for ϵ or ω, was needed, since the additional length scale of the filter, Δ, is already available. Deardorff concluded that there was no gain in retaining the residual stress equations, but there was gain in keeping the residual kinetic energy equation, especially for stably-stratified boundary layers. He retained the residual kinetic energy in his subsequent work, as have many others, especially in the atmospheric sciences.

The argument for including the k-ϵ or Reynolds stress equations in RANS is that the turbulence and mean flow can develop on different time scales. For example, when the equation for k is included, with $a_{ij} = -2\nu_T\langle S_{ij}\rangle$, $\nu_T = ck^{1/2}\ell$, then a_{ij} and hence the Reynolds stress can develop on a different time scale from that of $\langle S_{ij}\rangle$. For large-eddy simulations of high Reynolds number flows, with the filter length Δ in the inertial subrange, the residual scales may be in approximate equilibrium, and not evolve on their own time scale. The residual scales 'immediately' respond to changes in the large-scale motions. So in this case computing a separate equation for the residual scales may not be useful. For lower bandwidth large-eddy simulations, however, where Δ is not in the inertial subrange, which is usually the case for large-eddy simulations today, the computation of a separate equation for residual scale motions may be useful, especially since the residual scales will probably not be in equilibrium.

Some test were done by Steve de Bruyn Kops here at the University of Washington, who accurately simulated the homogeneous decay experiments of Comte-Bellot and Corrsin using 512^3 grid points. When he then performed an *a priori* test by filtering his results down to 128^3 grid points and examined the motions which had been filtered out, he found that the residual scale motions were not in equilibrium; in particular, the energy flux into the subgrid-scales was not equal to the energy dissipation rate (see Equation (29)). This is not a definitive test, however, as no inertial subrange existed in this flow.

The equation for the subgrid-scale motions has been previously derived, see Equation (28), and some comments about it already made. When it is used in large-eddy simulations, it is generally modeled as:

$$\frac{\partial}{\partial t}k_r + \bar{U}_j\frac{\partial}{\partial x_j}k_r = -\frac{\partial}{\partial x_j}q_j^k - \epsilon^k - \tau_{ij}^r\bar{S}_{ij}\,,$$

with $\epsilon^k = c_\epsilon\dfrac{k_r^{3/2}}{\Delta}$, $q_j^k = 2P_r^{-1}\nu_r\dfrac{\partial}{\partial x_j}k_r$, $P_r = \nu_r/D_r$ with ν_r the sgs viscosity, c_ϵ estimated to be 0.93 (see exercise 13.45 in the text), and the residual Prandtl number take to be $P_r \doteq 1$.

8 Other residual stress models

There are a number of other residual stress models (and the number is increasing almost daily). Some of the more important ones will be mentioned here.

8.1 Hyperviscosity

The use of hyperviscosity is sometimes called a 'poor man's LES', and is often used in geophysical fluid dynamics. The idea is to write the momentum equation as:

$$\frac{\partial}{\partial t}U_i + U_j\frac{\partial}{\partial x_j}U_i = -\frac{1}{\rho}\frac{\partial P}{\partial x_i} + \nu_h(-1)^{m+1}\nabla^{2m}U_i\,,$$

where m is an integer with $m > 1$. (If $m = 1$ this reduces to the usual incompressible form of the Navier-Stokes equations.) To understand this method, it is better to examine the equation for the Fourier amplitude of U_i, say $\hat{U}(\mathbf{k}, t)$, i.e.,

$$\frac{\partial}{\partial t}\hat{U}_i(\mathbf{k},t) = \underbrace{\mathcal{N}_i}_{\substack{\text{transform of}\\ \text{nonlinear and}\\ \text{pressure terms}}} + (-1)^{m+1}(i)^{2m}\nu_h(k_j^2)^m\hat{U}_i(\mathbf{k},t)\,,$$

or, with $(i)^{2m} = (-1)^m$, so that $(i)^{2m}(-1)^{2m+1} = -1$, $k^2 = k_jk_j$,

$$\frac{\partial}{\partial t}\hat{U}_i(\mathbf{k},t) = \mathcal{N}_i - \nu_h k^{2m}\hat{U}_i(\mathbf{k},t) = \mathcal{N}_i - \underbrace{\nu_h k^{2(m-1)}}_{\nu_r}k^2\hat{U}_i(\mathbf{k},t)\,. \tag{45}$$

So the effictive 'residual scale' viscosity is now $\nu_r = \nu_h k^{2(m-1)}$. Figure 19 has plots of $\nu_r/(\nu_h k_c^{2(m-1)})$ versus k/k_c for $m = 1$, 2, or 3, and where k_c is a truncation wave number. Note that as m is increased, the effects of the hyperviscosity decreases at low wave numbers, but increases near the wave number cutoff.

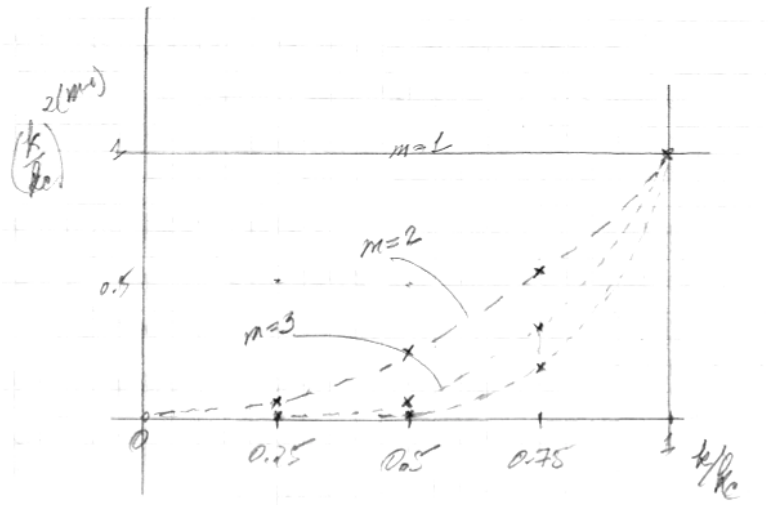

Figure 19: Plot of the normalized hyperviscosity for several different values of m.

The spectral energy equation, obtained by multiplying Equation (45) by the complex conjugate of $\hat{U}_i$, taking the complex conjugate of (45) and multiply by $\hat{U}_i$, adding the two resulting equations and dividing by 2, is

$$\frac{\partial}{\partial t}\frac{1}{2}|\hat{U}_i|^2 = \underbrace{\mathcal{T}}_{\substack{\text{conservative,}\\ \text{spectral energy}\\ \text{transfer}}} - \nu_h k^{2(m-1)}k^2|\hat{U}_i|^2\,.$$

So as m is increased, the large-scale motions become effectively inviscid, as they should in a high Reynolds number flow, and dissipation occurs at the smallest scales. Therefore using hyperviscosity gives the qualitative features of Smagorinsky's model.

This approach is very easy to implement, especially with spectral numerical methods, with almost no computational overhead. The assumptions in the model are very clear. Some experimentation is required, however, for the choices of ν_h anf m for a particular problem, as these can vary from problem to problem.

8.2 Monotone integrated large-eddy simulation (MILES)

A number of numerical schemes have been developed which allow steep gradients (small scales) to develop, but which remain numerically stable. Most of these schemes, called monotone schemes, were developed to treat shocks and contact surfaces, which are essentially discontinuities. The first is called 'flux correction' (Boris & Book); others are the total variation diminishing (TVD) scheme, Godunov's scheme, and probably more. All of these allow large-scale motions to evolve somewhat inviscidly, while energy is being extracted at the smallest scales. The schemes are actually highly nonlinear filters. The methods are fairly easy to implement, and without much additional computational overhead. Damping (viscous) is only applied when and where necessary, when steep gradients develop. How consistent the modeling is with residual stresses is unclear.

8.3 Deconvolution, or defiltering

A method that is gaining in popuularity is called deconvolution, or defiltering. It is based upon operations at the small scales. The original idea was to invert the filtering due to the numerical method, and use the result as a subgrid-scale model. Later what has been done is to invert or deconvolve the filter used in the large-eddy simulation, and use this result as a subgrid-scale model.

8.4 Mechanistic-based models

Another class of subgrid-scale models are mechanistically based, i.e., a physical model for the subgrid-scale motions is hypothesized, then implemented in some mathematical/numerical manner. Among these are:

- the linear-eddy model (LEM), and its descendent the one-dimensional turbulence (ODT) model (Kerstein). This model treats the subgrid-scales as a series of one-dimensional maps, the type of mapping and the rate of application consistent with some of the properties of the subgrid-scale turbulence.

- the stretched-vortex model (Saffman, Pullin). In this model the subgrid-scale motions are considered to be an agglomeration of randomly oriented vortices, which are stretched and rotated by the larger-scale flow. There is much mathematical analysis used in deriving the model, with a number of simplifying assumptions.

- Monte-Carlo based models used in the filtered Probability Density Function (PDF) approach; this is an extension of an approach also used in RANS, and will be described next in the course.

8.5 Very large-eddy simulations (VLES)

In this approach there is no pretense that the filter scale Δ is in the inertial subrange, but is at much larger scales. A significant amount of the energy is filtered out, and it becomes more important to

employ a dynamic equation for the subgrid scales, for example for k_r. The approach still contains more physics that RANS, as the larger-scale turbulent motions are still directly computed, whereas in RANS these motions have been averaged out and must be modeled. Many large-eddy simulations carried out today are actually VLES, due to the lack of resolution.

8.6 Unsteady RANS

RANS modeling has been developed and validated for statistically steady flows. There are a number of turbulent flows, however, to which it is applied, for example, internal combustion engines, cardiovascular flows, and many geophysical fluid dynamics flows (codes such as ROMS (Regional Ocean Modeling System) contain RANS models for the smaller-scale turbulence). Note that the RANS 'constants' have been adjusted to agree with statistically steady flows, and may needed some readjustment for unsteady ones. Also, unsteadiness can bring in some new physics, which is not modeled in RANS models developed for statistically steady flows. For example, flow acceleration tends to stabilize flows, while deceleration tends to destabilize them; both of these affect the turbulence, but are not included in the usual RANS modeling.